

Acceleration of injected electrons in a laser wakefield experiment

F. Dorchies, F. Amiranoff, V. Malka, J. R. Marquès, and A. Modena
*Laboratoire pour l'Utilisation des Lasers Intenses, UMR n°7605, CNRS-CEA-Ecole
 Polytechnique-Université Paris VI, Ecole Polytechnique, 91128 Palaiseau, France*

D. Bernard, F. Jacquet, and Ph. Miné
*Laboratoire de Physique Nucléaire et des Hautes Energies, IN2P3-CNRS, Ecole Polytechnique,
 91128 Palaiseau, France*

B. Cros and G. Matthieussent
Laboratoire de Physique des Gaz et des Plasmas, CNRS, Université Paris XI, 91405 Orsay, France

P. Mora and A. Solodov
Centre de Physique Théorique, CNRS, Ecole Polytechnique, 91128 Palaiseau, France

J. Morillo
*Laboratoire des Solides Irradiés, UMR n°7605, CNRS-CEA/DSM/DRECAM-Ecole Polytechnique,
 91128 Palaiseau, France*

Z. Najmudin
Blackett Laboratory, Imperial College, SW7 2AZ London, United Kingdom

(Received 14 January 1999; accepted 17 March 1999)

An electron plasma wave (EPW) has been excited by a short laser pulse (5 J, 400 fs) via the laser wakefield (LWF) mechanism. At the LWF quasi-resonance condition, the 3 MeV injected electrons have been accelerated with a maximum energy gain of 1.5 MeV. The maximum longitudinal electric field is estimated to be 1.5 GV/m. It has been observed that electrons deflected during the interaction, can scatter on the walls of the experimental chamber and fake a high energy signal. A special effort has been given in the electron detection to separate the accelerated electrons signal from the background noise. The experimental data are confirmed with numerical simulations, demonstrating that the energy gain is affected by the EPW radial electric field. The duration of the EPW inferred by the number of accelerated electrons and by the numerical simulations is of the order of 1–10 ps. © 1999 American Institute of Physics. [S1070-664X(99)00107-X]

I. INTRODUCTION

The accelerating electric field (or gradient) in conventional radio frequency linear accelerators is limited to around 100 MV/m, partly due to heating or breakdown on the walls of the structure. In order to accelerate electrons to very high energies (>1 TeV) without building a too long and too expensive structure, it is necessary to develop new acceleration concepts providing a higher accelerating electric field. In this context, plasma-based accelerators are of great interest because plasmas can sustain very high electric fields. More precisely, the longitudinal electric field associated with an electron plasma wave (EPW) can reach more than 100 GV/m with a phase velocity close to the speed of light c , making it very attractive for relativistic electron acceleration.¹ In several experiments,¹ such an EPW has been excited by an electron beam propagating in a plasma, but the gradients obtained were relatively low (<30 MV/m). Tajima and Dawson² proposed to use the ponderomotive force associated with a laser pulse to excite an EPW. Two mechanisms were considered.

The laser beat wave (LBW) mechanism consists in mixing two laser beams with different pulsations ω_1 and ω_2 . Their beating provides a modulation of the light intensity at the pulsation $\omega_b = \omega_1 - \omega_2$. When ω_b is equal to the electron

plasma pulsation ω_p , an EPW is resonantly excited. LBW acceleration has been observed and studied in several experiments with 1 (Ref. 3) and 10 μm (Refs. 4–6) lasers. It has been experimentally demonstrated that this mechanism could be affected by different saturation mechanisms: relativistic detuning⁵ or modulational instability.⁷

In the laser wake field (LWF) approach,^{8,9} a single short laser pulse excites the EPW: the ponderomotive force associated with the front (then the rear) of the laser pulse pushes the plasma electrons in the forward direction (then in the backward direction). The EPW excitation is the most efficient when the laser pulse duration is of the order of $1/\omega_p$. This “quasi-resonance” is not as strict as the LBW resonance. Moreover, the LWF EPW excitation is achieved in a time ($1/\omega_p$) which is generally very short with regard to the typical evolution time ($1/\omega_{pi}$) of the plasma ions [$\omega_{pi}/\omega_p = (Zm_e/m_i)^{1/2} \ll 1$, where m_e is the electron mass, m_i the ion mass and Z the plasma ionization state]. So the LWF process should not be affected by saturation as is LBW.

Another regime, called the self modulated laser wake field (SMLWF), has been considered recently.^{10–12} An ultraintense laser pulse with duration longer than $1/\omega_p$, can be temporally modulated at the plasma pulsation ω_p via the

stimulated Raman forward (and side) scattering instability. The EPW is then self-resonantly excited by this laser intensity modulation. If the excited longitudinal electric field is sufficiently high, plasma electrons can be trapped in the EPW and accelerated to high energies as it has been observed in recent experiments.^{13–17} With the same laser pulse duration, the SMLWF regime operates at higher density than the “standard” LWF. The Lorentz factor $\gamma_p = \omega/\omega_p$ of the EPW phase velocity is then lower, making this regime not well suited for high energy accelerators. Moreover, since in this case the EPW is generated by an instability, its phase cannot be controlled.

LWF seems to be the best candidate for particle acceleration to high energy. Within the last few years, the chirped pulse amplification (CPA) technique¹⁸ has allowed the development of sources delivering the ultrashort and intense laser pulses needed for LWF experiments. The first experimental evidence for plasma wave generation by the LWF mechanism was obtained in a strongly radial regime by Hamster *et al.*¹⁹ Recently, the excitation of radial EPW by LWF has been extensively studied, using frequency domain interferometry.^{20–22}

In this paper, we present the first experimental study of LWF acceleration of injected electrons. Accelerated electrons were observed at the EPW output when the “quasi-resonance” condition was realized, confirming the LWF acceleration mechanism. The experimental results were confirmed with three-dimensional (3D) simulations, demonstrating that the energy gain is affected by the EPW radial electric field.

In previous LBW acceleration experiments, Clayton *et al.* demonstrated that electrons could be deflected a relatively long time (a few nanoseconds) after the EPW excitation, by transverse electric and/or magnetic fields due to a Weibel-like instability.²³ These deflected electrons can scatter on the walls of the experimental chamber and fake accelerated electron signals, as is probably the case in the contested results of Ref. 24. Thus, in our experiment, a special care was taken to separate the accelerated electrons signal from the background noise, both in the design of the experimental apparatus and in the data analysis.

II. LWF LINEAR MODEL

Gorbunov and Kirsanov have developed a two-dimensional (2D), nonrelativistic analytical model of the LWF.⁸ The plasma electrons are described by cold fluid equations with the ponderomotive potential term induced by the laser pulse spatial and temporal profiles. Ions are assumed to be fixed during the EPW excitation. Equations are solved assuming that the electron density perturbation δn is small compared with the equilibrium electron density n_e (linear approximation), and that the spatial (radial) and temporal parts of the ponderomotive potential can be separated. This condition is achieved with a gaussian beam, since the Rayleigh length $z_R = 2\pi\sigma^2/\lambda$ (2 mm in our experiment) is much longer than the pulse length $c\tau$ (of the order of 100 μm). λ is

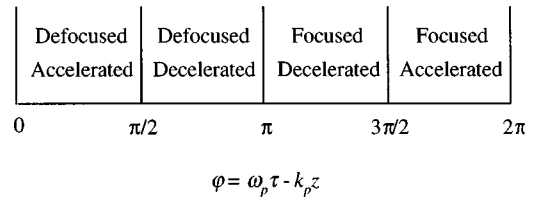


FIG. 1. Depending of its relative phase $\varphi = \omega_p \tau - k_p z$ with the EPW, an injected electron is accelerated or decelerated by E_z , and focused or defocused by E_r .

the central wavelength, σ is the focal spot radius, and τ is the duration defined so that the laser intensity I can be expressed in the vicinity of the focus as

$$I(z, r, t) = I_{\max} e^{-(r/\sigma)^2} e^{-[(t-z/c)/\tau]^2}.$$

The electron density perturbation excited by the pulse is then given by

$$\begin{aligned} \frac{\delta n}{n_e} &= \frac{\delta n_z}{n_e} + \frac{\delta n_r}{n_e} \\ &= -A \left[1 + \left(\frac{\lambda_p}{\pi\sigma} \right)^2 \left(1 - \frac{r^2}{\sigma^2} \right) \right] \times e^{-r^2/\sigma^2} \sin(\omega_p t - k_p z), \end{aligned}$$

where

$$A = \frac{I_{\max} \sqrt{\pi}}{c^3 n_c m_e} \left(\frac{\omega_p \tau}{2} \right)^2 e^{-(\omega_p \tau/2)^2},$$

n_c is the critical density at the laser wavelength λ , and λ_p is the plasma wavelength ($\lambda_p = 2\pi/k_p = 2\pi c/\omega_p$ since the group velocity of the laser pulse is very close to c in an underdense plasma, $n_e \ll n_c$).

The longitudinal contribution δn_z corresponds to longitudinal electron oscillations. The electric field E_z deduced from δn_z by the Poisson equation is also longitudinal. The radial contribution δn_r corresponds to cylindrical electron oscillations associated with a radial electric field E_r . These electric fields are given by

$$E_z = \xi \cos(\omega_p t - k_p z),$$

$$E_r = \xi \left(\frac{\lambda_p}{\pi\sigma} \right) \left(\frac{r}{\sigma} \right) \sin(\omega_p t - k_p z)$$

with

$$\xi = \frac{2I_{\max} \sqrt{\pi}}{e c^2 n_c \tau} \left(\frac{\omega_p \tau}{2} \right)^2 e^{-(\omega_p \tau/2)^2} e^{-r^2/\sigma^2},$$

where e is the elementary charge.

Depending of its relative phase $\varphi = \omega_p \tau - k_p z$ with respect to the EPW, an injected electron is accelerated or decelerated by E_z , and focused or defocused by E_r (see Fig. 1). Only a quarter of the EPW cycle is both accelerating and focusing ($3\pi/2 < \varphi < 2\pi$).

The distinction between the radial and the longitudinal regime of the LWF is often estimated by the ratio $\delta n_r/\delta n_z = (\lambda_p/\pi\sigma)^2$. In an acceleration experiment, the important

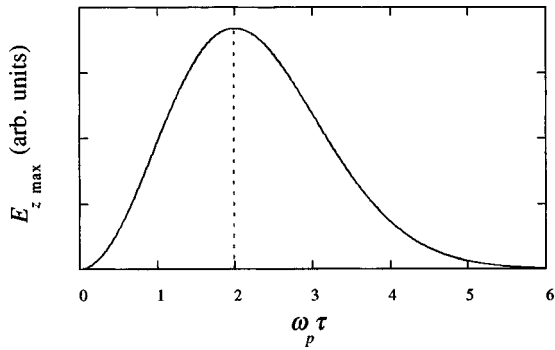


FIG. 2. LWF quasi-resonance. Amplitude of the longitudinal electric field $E_{z,\max}$ associated with the EPW, as a function of the product $\omega_p \tau$ (the laser duration τ is fixed).

parameters are the maximum amplitudes of radial ($E_{r,\max}$, reached at $r = \sigma/\sqrt{2}$) and longitudinal ($E_{z,\max}$, reached at $r = 0$) electric fields. Their ratio is equal to $(\lambda_p/\pi\sigma)/\sqrt{2e}$.

Figure 2 represents $E_{z,\max}$ as a function of the product $\omega_p \tau$, with a given laser duration τ . It is maximum when the quasi-resonance condition $\omega_p \tau = 2$ is realized. Because $\omega_p = (n_e e^2/m_e \epsilon_0)^{1/2}$, this condition can be satisfied by adjusting the mean electron density n_e . At this quasi-resonance, the longitudinal electric field is given by

$$E_{z,\max}(\text{GV/m}) = 0.82 \frac{\lambda^2(\mu\text{m}) I_{\max}(10^{18} \text{ W cm}^{-2})}{\tau(\text{ps})}.$$

It is proportional to the laser energy E_{las} , and inversely proportional to the square of the laser duration.

With our typical experimental parameters [$\tau = 240$ fs (400 fs full width at half maximum—FWHM), $\sigma = 18 \mu\text{m}$, $I_{\max} = 4 \times 10^{17} \text{ W cm}^{-2}$], the above linear model leads to: $n_e = 2.2 \times 10^{16} \text{ cm}^{-3}$ (electron density at the quasi-resonance), $\lambda_p = 225 \mu\text{m}$, $\delta n_z/n_e = 11\%$, $E_{\max} = 1.5 \text{ GV/m}$, $\delta_r/n_e = 175\%$, $E_{r,\max} = 2.6 \text{ GV/m}$, and $\delta n_r/\delta n_z = 16$, indicating that the EPW excitation occurs mainly in the radial regime: the transverse field is stronger than the longitudinal electric field. The relative density perturbation is well above the linear approximation given by $\delta n/n_e \ll 1$. In order to check the validity of the linear expression for the longitudinal electric field E_z , numerical simulations were performed with the fully relativistic 2D (cylindrical) particle code WAKE.²⁵ The parameters were close to the experimental values: $E_{\text{las}} = 3 \text{ J}$, 350 fs FWHM, and the corresponding mean electron density at the quasi-resonance $n_e = 2.84 \times 10^{16} \text{ cm}^{-3}$. The calculation was performed for different values of σ , inducing different values of $\delta n_r/n_e$. Figure 3 shows the amplitude of the calculated longitudinal electric field $E_{z,\text{sim}}$ normalized to the linear model expression $E_{z,\max}$, as a function of $\delta n_r/n_e$ ($\delta n_r/n_e$ is estimated with the linear model). The longitudinal electric field is observed to be in good agreement with the linear value for $\delta n_r/n_e < 2$ (corresponding to $\delta n_z/n_e < 0.2$). Beyond this value, the nonlinearities of the EPW induce the relative decrease of the longitudinal electric field. With a higher energy (10 J), the transition between these two regimes is still observed close to $\delta n_r/n_e = 2$ (corresponding then to $\delta n_z/n_e < 0.4$). These simulations show that the LWF linear model is valid for our experimental parameters.

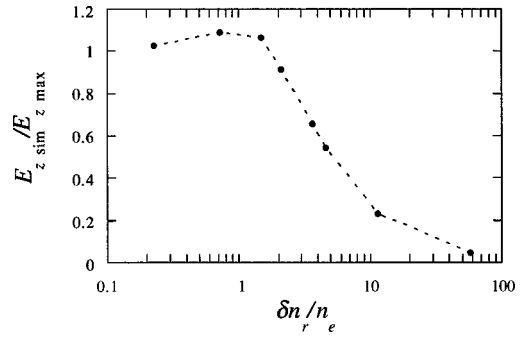


FIG. 3. Amplitude of the longitudinal electric field $E_{z,\text{sim}}$ as a function of $\delta n_r/n_e$. It is calculated at the quasi-resonance with the code WAKE and is normalized to its expression $E_{z,\max}$ obtained from the LWF linear model. The laser energy is 3 J, its duration 350 fs FWHM and the electron mean density is $n_e = 2.84 \times 10^{16} \text{ cm}^{-3}$. The different values of $\delta n_r/n_e$ are obtained by varying the value of the laser focal spot radius σ .

Assuming that the EPW is infinite in the longitudinal direction, the energy gain ΔW of an electron injected on the laser axis is limited by $eE_{z,\max}L_d$, where L_d is the detuning length of the electron. In the case of our experiment, Lorentz factor of the injected electrons $\gamma_e = 6$ was very small compared to the EPW Lorentz factor at the quasi-resonance $\gamma_p = \lambda_p/\lambda = 215$. Assuming that the electron velocity was constant during the interaction and neglecting defocusing effects [one dimensional (1D) case], L_d is given by $L_d = \gamma_e^2 \lambda_p = 8 \text{ mm}$.²⁶ In fact, the EPW was only existing in the region of high laser intensity, i.e., typically over a length $\pi z_R = 6 \text{ mm}$. The energy gain was then limited to $eE_{z,\max}\pi z_R = 9 \text{ MeV}$. A more precise value is obtained with a one-dimensional Monte Carlo simulation of the electron trajectories in the EPW electric field. The electric field E_z is calculated from the LWF linear model. To describe the longitudinal dependence of its envelope, the laser beam is assumed to be gaussian. The intensity around the focus plane $z = 0$ is given by

$$I(z) = \frac{I_{\max}}{1 + (z/z_R)^2}$$

and the longitudinal electric field is

$$E_z(z,t) = \frac{E_{z,\max}}{1 + (z/z_R)^2} \cos(\omega_p t - k_p z).$$

In the simulation, 1000 electrons are injected with a uniform phase distribution. Figure 4 shows the energy gain ΔW calculated as a function of the injection phase φ . Accelerating and decelerating phases are well delimited. The maximum energy gain is about $\Delta W_{\max} = 7.5 \text{ MeV}$.

III. EXPERIMENTAL SETUP

The experimental setup was based on the existing facility already used for LBW experiments. It is exhaustively described in Ref. 27. The modified setup used in the experiment which we present in this paper, is sketched in Fig. 5. The laser beam was focused into a gas vessel and created a plasma close to focus. The electron beam was injected into the gas vessel through a thin aluminum window, and was

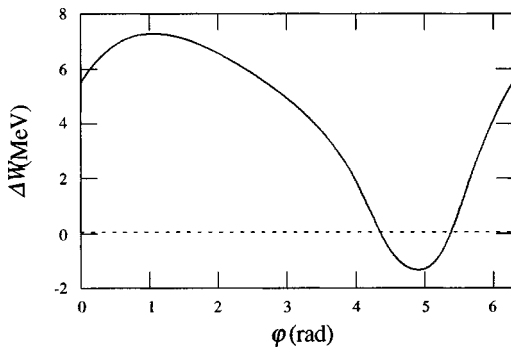


FIG. 4. 1D Monte Carlo simulation of the energy gain ΔW of 1000 injected electrons as a function of their injection phase φ with respect to the EPW. The EPW electric field is given by the linear model with the experimental parameters of Table I. φ is defined as the phase the electron would have without EPW at the focal plane.

focused on the laser focal plane by a triple focusing magnet. The two beams were precisely monitored and overlapped by placing a thin aluminum foil at the focal plane and by looking at the optical transition radiation of the electron beam and at the laser beam scattering. The momentum of the accelerated electrons was analyzed with a quadrupole-dipole magnetic spectrograph.

The electron beam was provided by a Van de Graaff accelerator, with a total energy of 3 MeV (i.e., kinetic energy of 2.5 MeV). The bunch duration was 0.4 ns with a peak current of $3.15 \pm 15 \mu\text{A}$, corresponding to about 2000 electrons per picosecond. Considering that the EPW lifetime is typically of the order of 1 ps, the number of accelerated electrons is quite low. The detectors used were sensitive to single electrons. The nonaccelerated electrons were sent into a beam dump. The accelerated electrons were counted in a detector with 17 channels (indexed by $i=1-17$), allowing detecting from 3.3 to 5.9 MeV total energy. Each channel was composed of a scintillator connected to a photomultiplier (PM). The photomultiplier signal was stored on an ana-

logical digital converter (ADC_i). Several channels were also recorded on an oscilloscope. The voltage of the PMs was adjusted so that the calibration factor was equal to 2.5 ADC counts per electron. The duration of the ADC gate was set to 20 ns.

We used the laser beam from the Laboratoire pour l'Utilisation des Lasers Intenses (LULI) 100 TW laser system delivering chirped pulses with 500 ps FWHM duration, and a central wavelength $\lambda = 1.057 \mu\text{m}$. During this experiment, the laser energy was limited to 10 J. The laser beam was imaged via a 190 m long vacuum pipe, from the laser room to the Laboratoire des Solides Irradiés (LSI) experimental room located near the electron source. The laser pulse was compressed just before focusing in the gas vessel (the laser compressor is not represented in Fig. 5). A small fraction of the energy (2%) was taken at the compressor output and sent to a single-shot second-order autocorrelator. The measured pulse duration was about 400 fs FWHM with an important shot-to-shot fluctuation (from 300 fs to 1 ps FWHM). The laser beam was focused with a 1.4 m focal length 30° off-axis parabola. The laser beam focal spot was imaged on a charge coupled device (CCD) camera. Figure 6 shows a focal spot measured in vacuum. The corresponding horizontal (σ_H) and vertical (σ_V) radii are $\sigma_H = 20 \mu\text{m}$ and $\sigma_V = 12 \mu\text{m}$ at $1/e$ of the laser intensity. This is close to the diffraction limit $\sigma_{\text{diff}} = 11 \mu\text{m}$ calculated for the 80 mm diameter homogeneous beam and the 1.4 m focal length. The ellipse defined by these radii (area equal to $2\pi\sigma_H\sigma_V$) contains 50% of the total energy. After accounting for the different losses induced by the laser transport inside the pipe, the temporal compression and the focusing, the final energy available in the interaction area was close to $E_{\text{las}} = 1.5 \text{ J}$. The estimated laser intensity at focus was then typically $I_{\text{max}} = 4 \times 10^{17} \text{ W cm}^{-2}$. Under vacuum, the beam was imaged on the focal spot monitor at different planes along the longitudinal axis. From these measurements, the Rayleigh length was estimated to be $z_R = 2.0 \pm 0.3 \text{ mm}$ (the laser intensity on

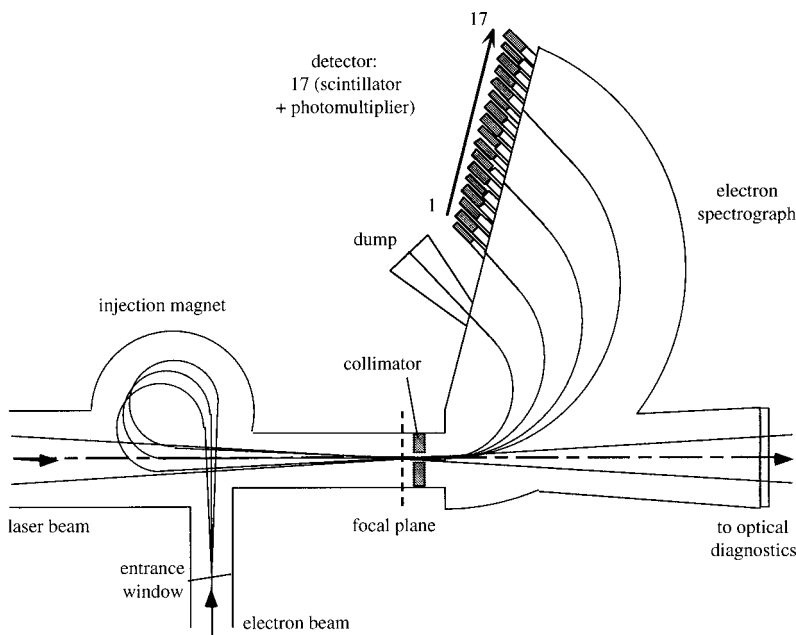


FIG. 5. Experimental setup.

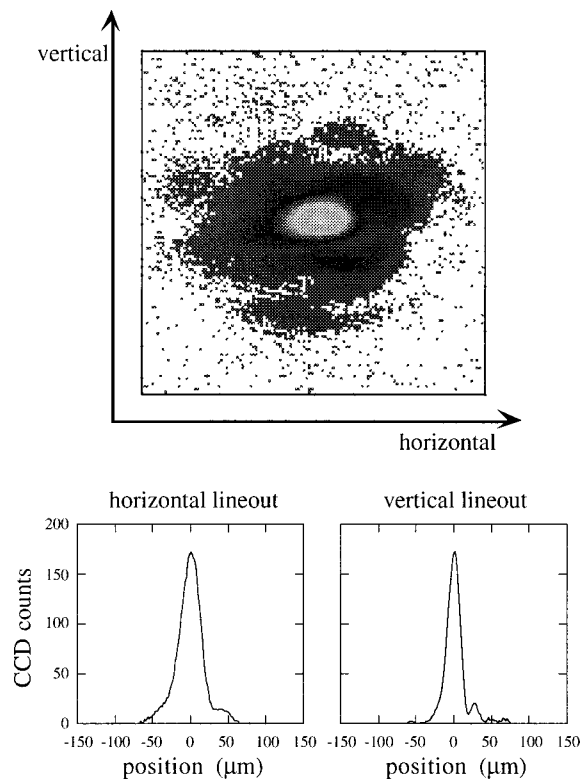
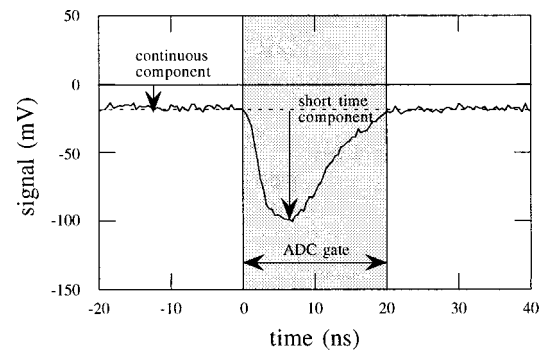


FIG. 6. Image of the laser focal spot, horizontal and vertical lineout.

the laser axis is divided by 2 after a propagation over z_R from the focal plane).

The experiment was performed focusing the laser in He gas at different pressures (0–4 mbar). The He^{2+} ionization intensity threshold is about $10^{16} \text{ W cm}^{-2}$ (Refs. 28, 29) and so, the interaction area can be considered as fully ionized. For pressures below 4 mbar, we observed that the ionization-induced refraction does not affect significantly the laser beam focal spot. From the laser duration value (400 fs FWHM), the LWF quasi-resonance is obtained for $n_e = 2.2 \times 10^{16} \text{ cm}^{-3}$, corresponding to 0.45 mbar of He gas. The parameters associated with the EPW are: the plasma wave-

FIG. 7. Oscilloscope trace of the PM_1 output signal during a “laser-electron-gas” shot. The shaded zone indicates the ADC temporal gate of integration (20 ns).

length $\lambda_p = 225 \mu\text{m}$, the plasma period $T_p = 2\pi/\omega_p = 750 \text{ fs}$, and the EPW Lorentz factor $\gamma_p = 215$. The experimental parameters are reported in Table I.

IV. EXPERIMENTAL RESULTS

We observed a signal on the electron detector on more than 200 shots. In order to check the temporal behavior of the electron signal, some PMs (PM_1 , PM_8 , and PM_{12}) were read both by an ADC and a fast oscilloscope. Figure 7 shows an oscilloscope trace recorded on PM_1 during a typical shot with laser, electron beam and He gas. Two different components are clearly separated. The short part ($< 20 \text{ ns}$, i.e., $< \text{ADC gate}$) of this trace is synchronized with the laser plasma interaction. It was only observed in presence of the laser, the electron beam and with He gas not too far from the quasi-resonance pressure. That is in agreement with the excitation of a large EPW. The other part of the trace contributing to the ADC integrated signal is continuous over the time scale of the detection. It was only observed in presence of gas. However, it was also observed in the absence of a laser pulse. Hence, it was only a product of the electron scattering in the gas. This “gas” background noise (“gas” BG noise) was separately and quantitatively studied as a function of He gas pressure, averaging 200 electron shots (at

TABLE I. Experimental parameters.

Electron beam injected		Laser (typical data)	
Total energy	3 MeV	Wavelength	1.057 μm
Lorentz factor	6	Energy in focus	1.5 J
Bunch duration	0.4 ms	Duration (FWHM)	400 fs
Divergence	10 mrad	Rayleigh length	2 mm
Spot size under vacuum (standard deviation)		Spot size under vacuum (radii in $1/e$ of intensity)	
horizontal	27 μm	horizontal	21 μm
vertical	24 μm	vertical	14 μm
Peak current	315 μA	Maximal intensity	$4 \times 10^{17} \text{ W cm}^{-2}$
Plasma & EPW (at LWF quasi-resonance)		Electron detection	
Electron mean density	$2.2 \times 10^{16} \text{ cm}^{-3}$	Number of channels	17
Lorentz factor	215	Energy range (tot. energy)	3.3–5.9 MeV
Plasma wavelength	225 μm		
Plasma period	750 fs		

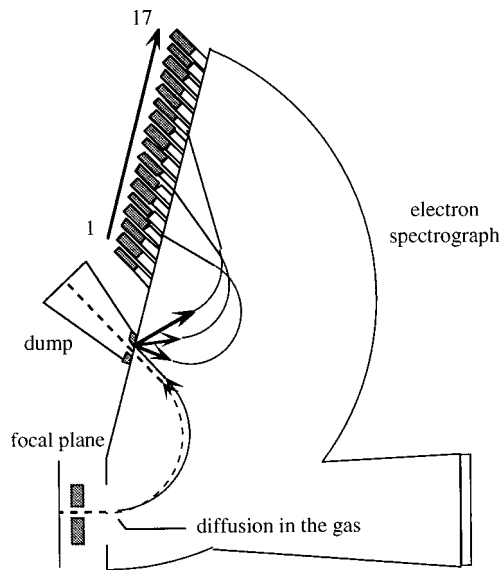


FIG. 8. "Gas" background noise source. A nondeflected 3 MeV electron goes into the dump (dashed line). If the electron is deflected in the gas, it can impact on the flange of the bottle neck of the dump and then be backscattered with a lower energy and give a signal on the detector (full lines).

10 Hz) for each pressure value. For a given pressure, we observed that the gas electron spectrum ("gas" BG noise as a function of the channel number) presented a very repetitive and relatively flat structure. Inserting stainless steel filters of different thicknesses in front of some channels, and comparing the observed transmission factor with the one calculated with the code EGS4 (Electron Gamma Shower),³⁰ the "gas" BG noise electron mean energy was estimated to be 2 MeV, independent of the channel number. This BG noise was observed to increase linearly with the He gas pressure with a slope of $8e^-/\text{mbar}$. It is caused by electrons deflected at low angle in the gas, that impact on the flange of the bottle neck of the dump (see Fig. 8). Part of these electrons are backscattered, re-enter the magnetic field of the spectrograph, and fly back into the detector. A numerical estimation of the amplitude of this noise was given in Ref. 27 and found to be in agreement with our measurements.

For all the "laser-electron-gas" shots around the quasi-resonance condition, electron signal was observed in excess of the "gas" BG noise. Figure 9 shows a typical electron spectrum ("EPW signal") obtained after the noise subtraction.

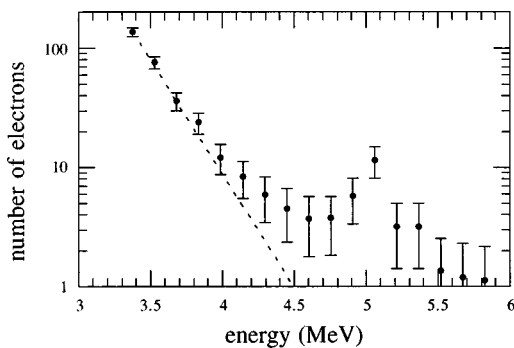


FIG. 9. Electron spectrum of a typical shot. The low energy points are fitted by a decreasing exponential.

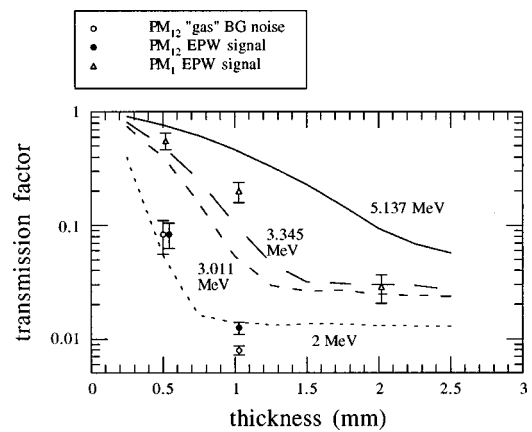


FIG. 10. Transmission factors of stainless steel filters measured on several channels as a function of the filter thickness. The lines are issued from a simulation described in the text. The nominal energy of PM_{12} (resp. PM_1) is 5.14 MeV (resp. 3.37 MeV).

tion. In the low energy range (from 3.3 to around 4.5 MeV), the number of electrons is well fitted by a decreasing exponential function. The associated slope was found equal to $-4.4 \pm 1.1 \text{ MeV}^{-1}$, for all the shots around $E_{\text{las}} = 1.5 \text{ J}$ with sufficiently high signal. In the higher energy range ($>4.5 \text{ MeV}$), a tail was observed with a structure similar to the subtracted "gas" BG noise. To check the actual energy of the detected electrons, stainless steel filters with different thicknesses were inserted in front of several channels. Figure 10 shows the transmission factors measured as a function of the filter thickness, as well as the transmission factors calculated with the code EGS4 (Ref. 30) for different electron energies. In the low energy range, the energy deduced from the transmission was in good agreement with the nominal energy of the corresponding channel, confirming the LWF electron acceleration. However, the high energy tail was produced by low energy electrons. The estimated energy of these electrons is around 2 MeV, corresponding to the mean energy of the "gas" BG noise electrons. This low energy signal (in the high energy channels) was observed into the 20 ns ADC gate and only for shots with accelerated electrons, that is in correlation with strong EPW excitation. Thus, we call it "EPW" BG noise. The deflection of the electrons by the EPW associated fields occurs in the electron focal plane, which is also the plane imaged by the magnetic field of the electron spectrograph on the detector input plane. A collimator placed at the entrance of the spectrograph stops the electrons deflected at angles larger than its angular acceptance. But some of the deflected electrons can scatter at the edge of the collimator, and impact on the flange of the bottle neck of the dump (see Fig. 11). Hence, the "EPW" BG noise produces the same structure and the same mean energy as the "gas" BG noise. This interpretation was confirmed by placing a thin Al foil ($11 \mu\text{m}$) at focus, under vacuum. The recorded electron spectrum associated with the electron beam deflection on the foil always reproduced the same structure. The "EPW" BG noise level is too high to be due only to the electrons deflected by the transverse electric field of the EPW, because of its short (ps) lifetime, and because of the high rejection power of the collimator system,²⁶ as dem-

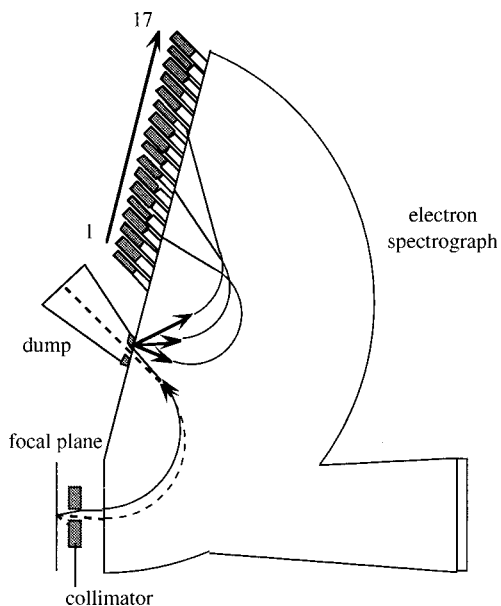


FIG. 11. “EPW” background noise source. Electrons deflected at the focal plane are imaged into the dump or stopped by the collimator (dashed lines). A few of them scatter on the edge of the collimator, and then impact on the flange of the bottle neck of the dump as is the case (see Fig. 8) for “gas” BG noise electrons (full lines).

onstrated by the low noise level induced by the foil. A long term (ns) effect like the Weibel instability, as previously observed in Ref. 23 is a good candidate to explain this BG.

Due to this “EPW” BG noise, we cannot measure precisely the maximal energy gain ΔW_{\max} of the accelerated electrons for a given electron spectrum. Thus, we have defined the maximum energy gain ΔW_{obs} as the value of the energy gain for which the decreasing exponential fit goes down to one electron. Since the slope of this fit was observed to be constant for all shots around $E_{\text{las}} = 1.5$ J, ΔW_{obs} was directly correlated to the signal observed on the PM_1 . For all these shots, the PM_1 signal is plotted in the Fig. 12 as a function of the product $\omega_p \tau$. ω_p is calculated from the He gas pressure, assuming a fully ionized plasma. τ is obtained from the single-shot autocorrelator traces. This plot indicates that the maximum signal could be reached only around the quasi-resonance condition $\omega_p \tau = 2$. The corresponding energy gain was $\Delta W_{\text{obs}} = 1.5$ MeV. The linear model (cf. II and

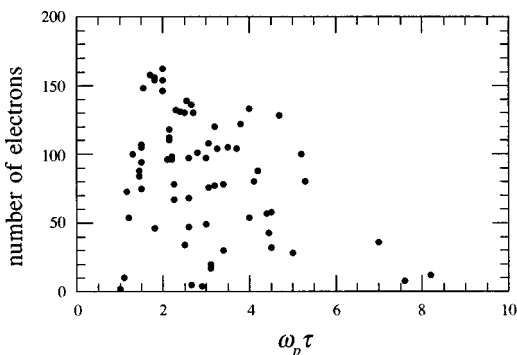


FIG. 12. Signal observed on the first channel (PM_1) as a function of the measured product $\omega_p \tau$. All shots performed with a laser energy around $E_{\text{las}} = 1.5$ J are reported.

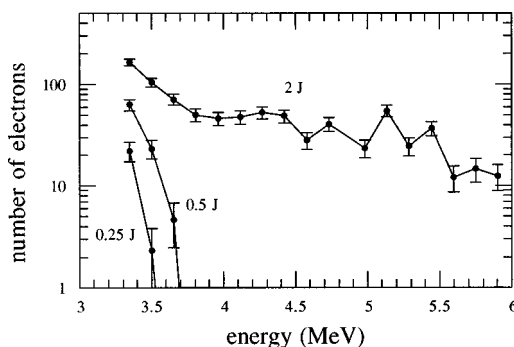


FIG. 13. Experimental electron spectra obtained with $E_{\text{las}} = 0.25, 0.5,$ and 2 J.

Fig. 2) indicates that the maximum value of the EPW longitudinal electric field at the quasi-resonance is proportional to E_{las}/τ^2 . The important fluctuation on the laser pulse duration (300 fs to 1 ps FWHM) leads to the dispersion of data points in the plot, more than the fluctuation on the laser energy E_{las} (1–2 J). This could be also a result of a lack of overlapping of the electron and laser beams.

Electron spectra were measured with different laser energies: 0.25, 0.5, and 2 J (see Fig. 13). The slope of the exponential fit is observed to increase (negative values) with the laser energy, as well as the number of electrons detected. The maximum value of the energy gain ΔW_{obs} exhibits the expected behavior of the LWF linear model.

V. SIMULATIONS AND DISCUSSION

In order to understand the shape of the electron spectra and the relatively low maximum energy gain (1.5 MeV instead of 7.5 MeV predicted by a 1D calculation using the LWF linear model), different numerical simulations were performed. We expect an important effect from the radial electric field E_r . In a first step, we have calculated the 3D trajectories of the injected electrons in the longitudinal and radial electric fields of the EPW. These fields were obtained from the LWF linear model and from our typical experimental parameters (see Table I). A Monte Carlo generator was used to create 1000 electrons with uniform distribution of injection phase ϕ in the EPW. Figure 14 shows the energy

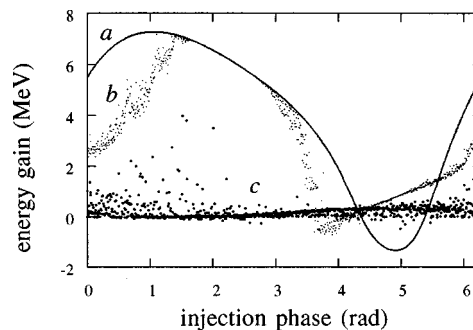


FIG. 14. 3D Monte Carlo simulation of the energy gain of 1000 injected electrons as a function of their injection phase ϕ in the EPW. Curve a: electron beam on axis (1D limit). Curve b: small emittance electron beam (30 nm \times 10 μ m std. dev.). Curve c: real emittance electron beam (30 μ m \times 10 mrad std. dev.).

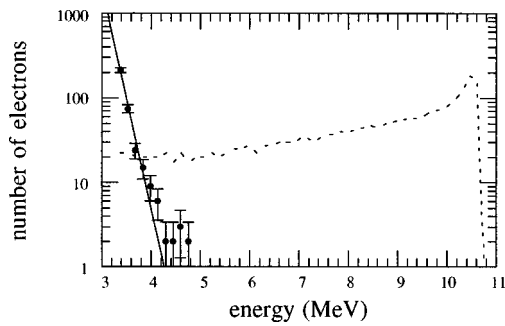


FIG. 15. Electron energy spectra obtained from the simulations of Fig. 12 (1000 electrons). Dotted line: in the 1D case (with arbitrary units for the number of electrons). Points: in the real emittance case (fitted by a decreasing exponential function).

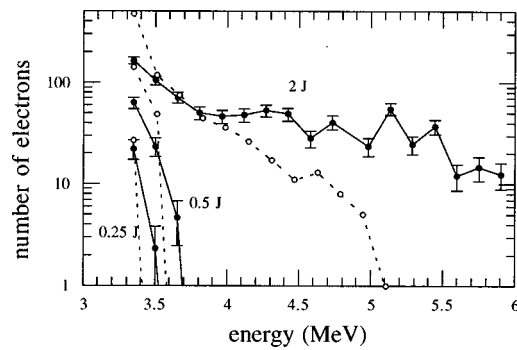


FIG. 16. Experimental electron spectra obtained with $E_{\text{las}}=0.25, 0.5,$ and 2 J (full lines), compared to the corresponding simulated spectra (dashed lines).

gain ΔW at the plasma output as a function of φ , for different electron beam emittances. Curve a is obtained with an electron beam on axis, that is nonaffected by the EPW radial electric field E_r . This is the simulation already presented in Fig. 4, which gives a maximum energy gain of 7.5 MeV. Curve b shows that even with a very small electron beam emittance (10^{-6} of the real emittance), the energy gain is affected by E_r . In the focusing phase domain of E_r , the energy gain is the same as in 1D simulation. But in the defocusing phase domain the electrons are deflected from the laser axis and go out of the accelerating region, decreasing their energy gain. Curve c is obtained with the experimental emittance. It shows that even in the focusing phase domain, the energy gain is lower than in the 1D case.

The energy spectrum deduced from the 1D calculated is plotted in Fig. 15. The maximum energy gain is well defined with the end of the spectrum at 7.5 MeV. The energy spectrum corresponding to the real emittance simulation is plotted on this same figure. It decreases exponentially with a slope of -6.1 MeV^{-1} , in good agreement with the experimental data. The maximum energy gain estimated with the

same method as for the experimental spectra is around 1.5 MeV. But, we note that the definition of the maximum energy gain obtained with this method depends a lot on the number of electrons simulated. Indeed, in the limit of an infinite number of simulated electrons, some electrons are exactly on the axis and can be accelerated to the maximum 1D value of 7.5 MeV. Simulations were performed with the three different laser energies associated with the spectra presented in Fig. 13. The electron spectra calculated are reported in Fig. 16, along with the experimental values. A good agreement is observed between the calculations and the experimental data. In the case of $E_{\text{las}}=2$ J, the ‘‘EPW’’ BG noise is important and contributes to the apparent difference between the two spectra.

Another simulation was performed, using the code WAKE²⁵ to calculate the EPW excitation and its evolution, using the experimental parameters (see Table I). As in the above simulations, 1000 electrons with a real emittance were injected in the EPW. The electron spectrum obtained is also very similar to the experimental one. Figure 17 shows the simulated evolution of the radial size of an electron bunch

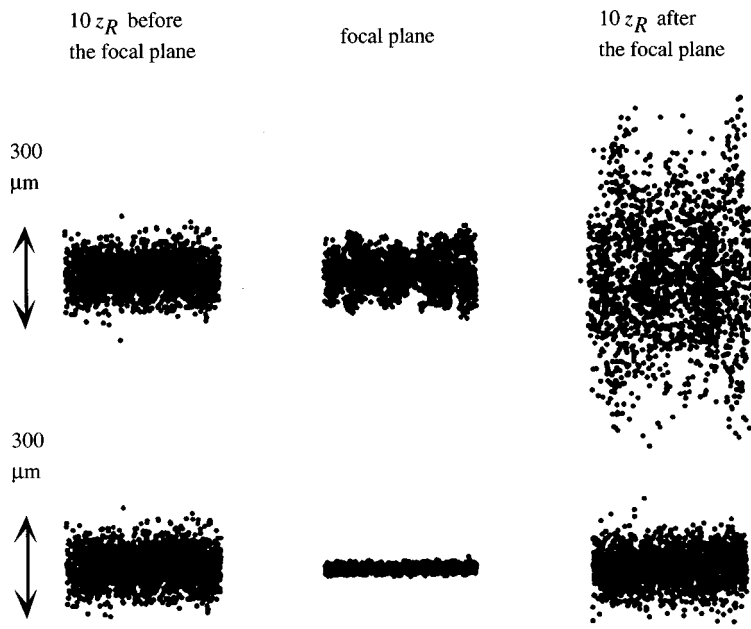


FIG. 17. Evolution of an electron bunch (3 ps duration) focused either under vacuum (bottom) or in the EPW (top): $10z_R$ before the focal plane, at the focal plane, and $10z_R$ after the focal plane. The longitudinal coordinate is the longitudinal position under the 3 ps bunch.

injected in the EPW, compared to the vacuum case (i.e., without EPW). The electron bunch duration is 3 ps (corresponding to four plasma periods at the LWF quasi-resonance). Under vacuum, the electron bunch is focused with a radius around $25 \mu\text{m}$ (std. dev.). The radius increases as the bunch leaves the focal plane. Its radius $10z_R$ after the focal plane is the same as that $10z_R$ before. In presence of the EPW, due to the strong radial electric field, the electron bunch cannot be as well focused as under vacuum: its focal plane radius is increased by a factor 5. Moreover, the electron beam explodes at the plasma output.

A simple analytical model³¹ describes the motion of an electron in an EPW with an infinite longitudinal dimension. Electrons in the defocusing phase are soon affected by the EPW radial electric field E_r and are expelled from the laser axis before entering the accelerating region (of the order of πz_R). The electron evolution in the focusing phase can be understood in three steps: a drift in free space, an ‘‘adiabatic’’ region where the electron is trapped by E_r and then another drift. The trapping by E_r occurs when the longitudinal relative amplitude $\delta n_z/n_e$ reaches the critical value $\delta_c = \gamma_e(\sigma/z_R)^2/2 = 2 \times 10^{-4}$ in our case (σ is the laser focal spot radius at $1/e$ of the intensity). That is at the distance z_c before the focal plane given by

$$z_c = z_R \sqrt{\frac{\delta n_{z\text{max}}/n_e}{\delta_c} - 1} \approx z_R \sqrt{\frac{\delta n_{z\text{max}}/n_e}{\delta_c}}$$

assuming a Gaussian laser beam. Since $\delta n_{z\text{max}}/n_e$ is close to 0.1 (i.e., 10%), the trapping occurs around $20z_R$ before the focal plane, that is well before the accelerating region (the efficient accelerating length is about πz_R). After the trapping, the electron oscillates rapidly in E_r , modifying the electron beam focusing. The electron beam radius σ_e (std. dev.) at the focal plane can be estimated by

$$\sigma_e = \frac{\sigma_{e0}}{\beta^*} \left(z_R \sqrt{\frac{\sigma n_{z\text{max}}/n_e}{\delta_c}} \right),$$

where σ_{e0} is the corresponding radius under vacuum, and β^* is the electron beam betatron function at focus under vacuum (2 mm in our experiment). From this expression and the experimental parameters, we deduce that σ_e is approximately equal to $5\sigma_{e0}$, i.e., around $125 \mu\text{m}$, in good agreement with the value obtained in the simulation presented in Fig. 17. Due to these oscillations on a transverse dimension larger than the transverse dimension of the accelerating area (i.e., σ around $17 \mu\text{m}$), the electron is not so exposed to the accelerating field as it would be the case without the radial electric field E_r , leading to a lower energy gain.

The E_r effect on an electron trajectory is actually more complicated. In the previous simple model, the electron phase in the EPW is considered not to change during its propagation in the EPW electric fields. In the case of our experiment, $\gamma_e = 6 \ll \gamma_p = 215$, so that the electron phase in the EPW decreases typically by π radians after a propagation over $4z_R$. Even if the electron is in a focusing phase at the focal plane, it is not the case a few z_R before the focal plane where the effect of the radial electric field is already influential. The electron can then be strongly expelled from the

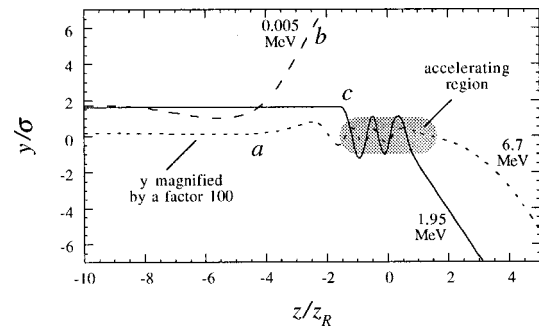


FIG. 18. Electron trajectories simulated with a linear model EPW. Initially, the electrons propagate collinearly with the laser axis at a distance of 30 nm (curve a), and $30 \mu\text{m}$ (curves b and c). Curve c is obtained with the EPW longitudinal size limited to πz_R around the focal plane (i.e., the EPW electric fields are set to zero out of the region $-\pi z_R/2 < z < \pi z_R/2$). The corresponding output energy gains are reported on the trajectories. The accelerating region defined by a longitudinal (resp. transverse) extend of πz_R (resp. 2σ) is also reported.

axis before entering on accelerating zone. Typical electron trajectories were calculated using a linear model EPW and our experimental parameters (see Fig. 18). The electron phase injection corresponds to 2 rad at the focal plane (i.e., 2 rad in Fig. 14), which is a focusing phase of the radial electric field E_r at this point. If the electron is close to the laser axis (curve a), its trajectory is not significantly modified by E_r , and its energy gain is high (6.7 MeV). If the electron is injected $30 \mu\text{m}$ from the laser axis (curve b), a few z_R before the focal plane the electron is in a defocusing phase of E_r . The electron is then deflected from the laser axis and miss the accelerating field, inducing a very low energy gain (0.005 MeV).

In order to increase the experimental energy gain to the 1D value with the same laser beam, various solutions can be proposed. The best proposal is to reduce the electron beam radius near the focal plane, in order to confine the electrons in the accelerating zone. The first solution would consist in using a more energetic electron beam. The critical value δ_c of the longitudinal relative amplitude would increase, and so the betatron oscillations due to trapping in the EPW would occur closer to the focal plane, where the electron beam radius would already be small enough. Moreover, due to the higher velocity of the electrons, the variation of their phase in the EPW fields during the propagation would be lower. Using the simple model of reference,³¹ reducing the trapping distance z_c to $\pi z_R/2$ would require in our experiment to inject a 375 MeV electron beam. Another solution would simply consist of reducing the EPW longitudinal dimension to the efficient acceleration length πz_R . This can be done, for example, by using a gas jet with an appropriate density profile dimension. Then the electron beam would not be affected by the EPW radial electric field before the accelerating region. Curve c in Fig. 18 shows an electron trajectory calculated with the same parameters than curve b, but with an EPW longitudinal dimension limited to πz_R . It clearly shows that (i) the electron enters and stays in the accelerating zone, (ii) its energy gain is quite higher (1.95 MeV) than in the nonlimited EPW case. In the same conditions, Fig. 19 shows the energy gain obtained as a function of the electron

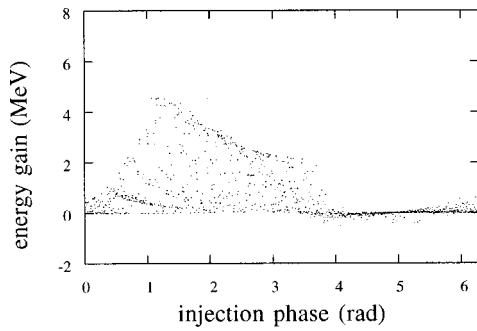


FIG. 19. 3D Monte Carlo simulation of the energy gain of 1000 injected electrons as a function of their injection phase φ in the EPW. The EPW longitudinal size is limited to πz_R around the focal plane. The electron beam emittance is the experimental one ($30 \mu\text{m} \times 10 \text{ mrad}$ std. dev.).

injection phase. The simulation parameters are the same as for Fig. 14 (curve c). The effect of the radial electric field on the injected electrons is observed to be clearly reduced. The corresponding electron spectrum (see Fig. 20) is closer to the 1D spectrum. Moreover, the maximum energy gain is well defined with the end of the spectrum at 4.5 MeV, corresponding to the longitudinal electric field of the linear model integrated over πz_R .

Assuming that the simulation presented in Fig. 15 describes correctly the experiment in terms of the ratio of accelerated electrons, we can deduce the EPW lifetime from the value of the electron beam current and from the number of electrons detected in the PM₁ both in the simulation and in the experiment. This estimation leads to a duration close to 1 ps. A simulation was performed with the code WAKE,²⁵ with the experimental parameters of Table I. The EPW longitudinal electric field E_z calculated as a function of time, is presented in Fig. 21. The deduced EPW lifetime is about 10 ps. The damping observed is correlated to the nonlinear radial amplitude of the density perturbation.²²

VI. CONCLUSION

We have demonstrated the acceleration of electrons injected in an electron plasma wave excited by the laser wake field mechanism. 3 MeV electrons were accelerated with a maximum energy gain of about 1.5 MeV, indicating an accelerating longitudinal electric field of about 1 GV/m. A tail was also observed in the higher energy channels. Measuring

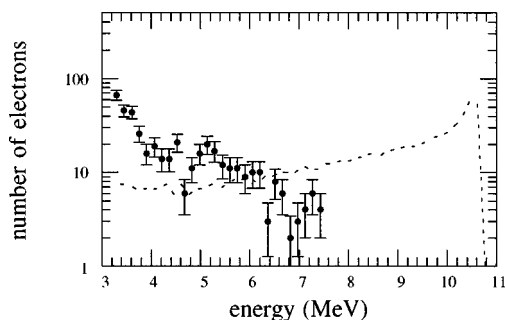


FIG. 20. Points: electron energy spectra obtained from the simulations of Fig. 19 (1000 electrons). Dotted line: in the 1D infinite plasma case (with arbitrary units for the number of electrons).

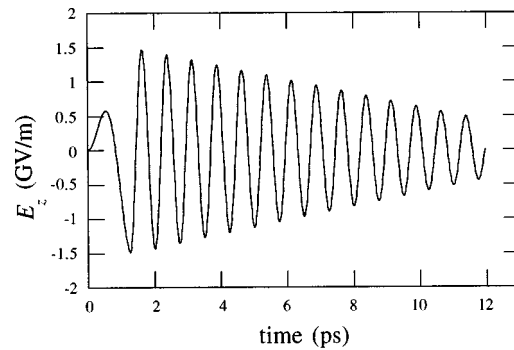


FIG. 21. EPW longitudinal electric field E_z calculated at the focal plane and on the laser axis, as a function of time. This calculation was performed with the code WAKE and the experimental parameters given in Table I. The time origin corresponds to 0.55 ps before the laser intensity maximum.

the transmission through stainless steel filters in front of the electron detector, we proved that this tail was actually due to low energy deflected electrons. This background noise, clearly correlated with the plasma wave excitation, can fake high energy accelerated electrons signal in such an experiment. We have inferred the EPW lifetime to be 1–10 ps from the experimental data and the simulations. The shape of the electron spectra as well as the maximum observed energy gain (1.5 MeV instead of 7.5 MeV estimated with a 1D calculation) were confirmed with 3D simulations, demonstrating that the electron beam focusing is modified by the strong radial electric field of the plasma wave, a long distance before the accelerating region. In order to reduce this negative influence, we propose the use of a gas jet to confine the EPW longitudinal size to the length of efficient acceleration. Simulations confirm that the electron beam focusing as well as the maximum energy gain, are then improved.

ACKNOWLEDGMENTS

It is a pleasure to acknowledge the help from the technical staff of the Laboratoire pour l'Utilisation des Lasers Intenses (LULI), Laboratoire de Physique Nucléaire et des Hautes Energies (LPNHE), Laboratoire des Solides Irradiés (LSI), and Commissariat à l'Énergie Atomique (CEA/DSM/DAPNIA-SEA) for this experiment. This work has been partially supported by Ecole Polytechnique, Institut National de Physique Nucléaire et de Physique des Particules (IN2P3), Centre National de la Recherche Scientifique (CNRS-SPI), and by the European Union (EU) Large Facility Program under Contract No. FMGE CT95 0044. The work of A. Solodov was supported in part by the Russian Basic Research Foundation (Grant Nos. 96-02-19482 98-02-17205).

¹E. Esarey, P. Sprangle, J. Krall, and A. Ting, *IEEE Trans. Plasma Sci.* **24**, 252 (1996).

²T. Tajima and J. Dawson, *Phys. Rev. Lett.* **43**, 267 (1979).

³F. Amiranoff, D. Bernard, B. Cros, F. Jacquet, G. Matthieussent, J. R. Marquès, Ph. Miné, P. Mora, A. Modena, J. Morillo, F. Moulin, Z. Najmudin, A. E. Specka, and C. Stenz, *IEEE Trans. Plasma Sci.* **24**, 296 (1996).

⁴Y. Kitagawa, T. Matsumoto, T. Minamihata, K. Sawai, K. Matsuo, K. Mima, K. Nishihara, H. Azechi, K. A. Tanaka, H. Takabe, and S. Nakai, *Phys. Rev. Lett.* **68**, 48 (1992).

- ⁵C. E. Clayton, K. A. Marsh, A. Dyson, M. Everett, A. Lal, W. P. Leemans, R. Williams, and C. Joshi, *Phys. Rev. Lett.* **70**, 37 (1993).
- ⁶N. A. Ebrahim, *J. Appl. Phys.* **76**, 7645 (1994).
- ⁷F. Moulin, F. Amiranoff, M. Laberge, J. R. Marquès, B. Cros, G. Matthieussent, D. Bernard, F. Jacquet, Ph. Miné, A. Specka, C. Stenz, and P. Mora, *Phys. Plasmas* **1**, 1318 (1994).
- ⁸L. M. Gorbunov and V. I. Kirsanov, *Zh. Eksp. Teor. Fiz.* **93**, 509 (1987).
- ⁹P. Sprangle, E. Esarey, A. Ting, and G. Joyce, *Appl. Phys. Lett.* **53**, 2146 (1988).
- ¹⁰N. E. Andreev, L. M. Gorbunov, V. I. Kirsanov, A. A. Pogosova, and R. R. Ramazashvili, *JETP Lett.* **55**, 571 (1992).
- ¹¹T. M. Antonsen and P. Mora, *Phys. Rev. Lett.* **69**, 2204 (1992).
- ¹²P. Sprangle, E. Esarey, J. Krall, and G. Joyce, *Phys. Rev. Lett.* **69**, 2200 (1992).
- ¹³A. Modena, Z. Najmudin, A. E. Dangor, C. E. Clayton, K. A. Marsh, C. Joshi, V. Malka, C. B. Darrow, C. Danson, D. Neely, and F. N. Walsh, *Nature (London)* **377**, 606 (1995).
- ¹⁴C. A. Coverdale, C. B. Darrow, C. D. Decker, W. B. Mori, K. C. Tzeng, K. A. Marsh, C. E. Clayton, and C. Joshi, *Phys. Rev. Lett.* **74**, 4659 (1995).
- ¹⁵K. Nakajima, D. Fisher, T. Kawakubo, H. Nakanishi, A. Ogata, Y. Kato, and Y. Kitagawa, *Phys. Rev. Lett.* **74**, 4428 (1995).
- ¹⁶D. Umstadter, S.-Y. Chen, A. Maksimchuk, G. Mourou, and R. Wagner, *Science* **273**, 472 (1996).
- ¹⁷D. Gordon, K. C. Tzeng, C. E. Clayton, A. E. Dangor, V. Malka, K. A. Marsh, A. Modena, W. B. Mori, P. Muggli, Z. Najmudin, D. Neely, C. Danson, and C. Joshi, *Phys. Rev. Lett.* **80**, 2133 (1998).
- ¹⁸D. Strickland and G. Mourou, *Opt. Commun.* **56**, 219 (1985).
- ¹⁹H. Hamster, A. Sullivan, S. Gordon, W. White, and R. W. Falcone, *Phys. Rev. Lett.* **71**, 2725 (1993).
- ²⁰J. R. Marquès, J. P. Geindre, F. Amiranoff, P. Audebert, J. C. Gauthier, A. Antonetti, and G. Grillon, *Phys. Rev. Lett.* **76**, 3566 (1996).
- ²¹C. W. Siders, S. P. L. Blanc, D. Fisher, T. Tajima, M. C. Downer, A. Babine, A. Stepanov, and A. Sergeev, *Phys. Rev. Lett.* **76**, 3570 (1996).
- ²²J. R. Marquès, F. Dorchies, F. Amiranoff, P. Audebert, J. C. Gauthier, J. P. Geindre, A. Antonetti, T. M. Antonsen, Jr., P. Chessa, and P. Mora, *Phys. Plasmas* **5**, 1162 (1998).
- ²³C. E. Clayton, M. J. Everett, A. Lal, D. Gordon, K. A. Marsh, and C. Joshi, *Phys. Plasmas* **1**, 1753 (1994).
- ²⁴M. Kando, H. Ahn, H. Dewa, H. Kotaki, H. Nakanishi, A. Ogata, T. Ueda, M. Uesaka, T. Watanabe, and K. Nakajima, *Phys. Rev. Lett.* (submitted).
- ²⁵P. Mora and T. M. Antonsen, Jr., *Phys. Plasmas* **4**, 217 (1997).
- ²⁶P. Mora and F. Amiranoff, *J. Appl. Phys.* **66**, 3476 (1989).
- ²⁷F. Amiranoff, J. Ardonneau, M. Bercher, D. Bernard, B. Cros, A. Debraine, J. M. Dieulot, J. Fusellier, F. Jacquet, J. M. Joly, M. Juillard, G. Matthieussent, P. Matricon, Ph. Miné, B. Montès, P. Mora, R. Morano, J. Morillo, F. Moulin, P. Poilleux, A. E. Specka, and C. Stenz, *Nucl. Instrum. Methods Phys. Res. A* **363**, 497 (1994).
- ²⁸M. V. Ammosov, N. B. Delone, and V. P. Krainov, *Sov. Phys. JETP* **64**, 1191 (1986).
- ²⁹S. Augst, D. Strickland, D. D. Meyerhofer, S. L. Chin, and J. H. Eberly, *Phys. Rev. Lett.* **63**, 2212 (1989).
- ³⁰See National Technical Information Service Document Nr. DE86007398 W. R. Nelson, H. Hirayama, and D. W. O. Rogers, *The EGS4 code system*, SLAC report 0265, Dec. 1985, p. 398. Copies can be ordered from the National Technical Information Service, Springfield, VA 22161.
- ³¹D. Bernard, *Nucl. Instrum. Methods Phys. Res. A* **410**, 418 (1998).